Theoretical Study of the $NH_2 + C_2H_2$ Reaction

L. V. Moskaleva and M. C. Lin*

Department of Chemistry, Emory University, Atlanta, Georgia 30322

Received: January 20, 1998; In Final Form: April 3, 1998

The potential energy surface of the amino radical reaction with acetylene has been studied by the ab initio molecular orbital method, and the reaction rate has been computed by a multichannel RRKM calculation. At the highest G2M(RCC) level of theory, the barrier height for the addition step was calculated to be 8.24 kcal/mol, producing solely the HCCH-trans amino-vinyl radical. The adduct can further undergo NH_2-for-H displacement decomposition and several isomerization reactions. The RRKM calculation was carried out for the lowest energy path, and the result indicates that the rate constant is expected to be pressure-dependent due to increased redissociation rate at low pressures. Kinetic modeling performed under experimental conditions reveals a substantial effect of secondary reactions on the observed NH_2 decay rates. This may explain the low activation energies reported for this reaction.

I. Introduction

The amidogen (or amino) radical, NH_2, is isoelectronic with CH_3 and OH. These radical species are relevant to fossil fuel combustion reactions. NH_2 plays a pivotal role in the thermal deNO_x process and in N-containing fuel chemistry.[1]

The reactions of NH_2 with hydrocarbons, particularly small unsaturated ones such as C_2H_2 and C_2H_4, are also important to the atmospheric chemistry of Jupiter and Saturn involving NH_3, CH_4, and their photochemical derivatives.[2,3] The mechanisms of these reactions have not been sufficiently characterized. For the reaction of interest to the present study, $NH_2 + C_2H_2$, four independent investigations employing different methods of reaction rate determination have been reported.[10−13] Hack et al.[12] first measured the rate constant by a discharge-flow/laser-induced fluorescence (DF/LIF) technique using He as carrier gas at 1 Torr pressure in the temperature range 210−505 K. The reported rate constant, $k = 1.42 \times 10^{16}T^{-2.70}$ cm^3/(mol·s), exhibits a strong negative temperature dependence. Bosco and co-workers,[13] on the other hand, observed a positive temperature dependence with $k = 6.68 \times 10^{10}e^{-1850/T}$ cm^3/(mol·s), employing a flash photolysis/laser-induced fluorescence (FP/LIF) method at 10−100 Torr (Ar dilution) in the temperature range 241−459 K. A similar study by Lesclaux and co-workers[10] used a flash photolysis/visible absorption (FP/VA) technique at 340−510 K with 30−100 Torr C_2H_2 without dilution. Their result, $k = 4.49 \times 10^{11}e^{-2780/T}$ cm^3/(mol·s), agrees reasonably well with that of Bosco, but differs significantly from that of Hack. More recently, Hennig and Wagner[11] investigated the reaction at high temperatures behind incident shock waves (1500−2000 K) at Ar pressures centering at ∼350 Torr. They reported $k = (3.7 \pm 0.4) \times 10^{12}e^{-5700/T}$ cm^3/(mol·s), giving the activation energy as high as 11.3 kcal/mol.

Theoretically, we must ask: What is the origin of the large scatter in the reported activation energies (which vary from ca. −5 to +11 kcal/mol) and what is the mechanism involved and the major products formed over the ranges of temperature and pressure investigated? To address these questions, we carried out detailed ab initio molecular orbital (MO) and RRKM calculations to elucidate the mechanism of the reaction and to calculate the rate constants for the formation of various products accessible at temperatures from 250 to 2500 K. In addition, we have performed kinetic modeling for the decay of NH_2 radicals under the conditions employed by Hack,[12] Stief,[13] Lesclaux[10] and co-workers to examine the potential effect of secondary reactions. The results of this investigation are presented herein.

II. Computation Procedure

A. Ab Initio MO Calculations. The G2M theoretical model employed in the present calculation, has been extensively described elsewhere.[5] The method modifies the original G2 technique[4] for applications to larger open shell systems.

The following is a brief description of the calculation procedure. The most elaborate RCC version of G2M has been employed, as recommended for systems with one to three heavy atoms. Accordingly, the geometries of all the reactants, products, and transition states were fully optimized using the hybrid density functional B3LYP method (Becke's three-parameter nonlocal exchange functional[6] with the nonlocal correlation functional of Lee, Yang, and Parr[7]) with the 6-311G-(d,p) basis set. Vibrational frequencies were obtained at the same level of theory for characterization of the nature of the stationary points and zero point energy (ZPE) corrections. The G2M(RCC) energy was calculated for each optimized structure as follows:[5]

$$E[\text{G2M(RCC)}] = E[\text{PMP4/6-311G(d,p)}] + \Delta E(+) + \Delta E(\text{2df,p}) + \Delta E(\text{RCC}) + \Delta' + \Delta E(\text{HLC}) + \text{ZPE[B3LYP/6-311G(d,p)]}$$

* Corresponding author. E-mail address: chemmcl@emory.edu.

S1089-5639(98)00823-8 CCC: $15.00
Published on Web 05/15/1998

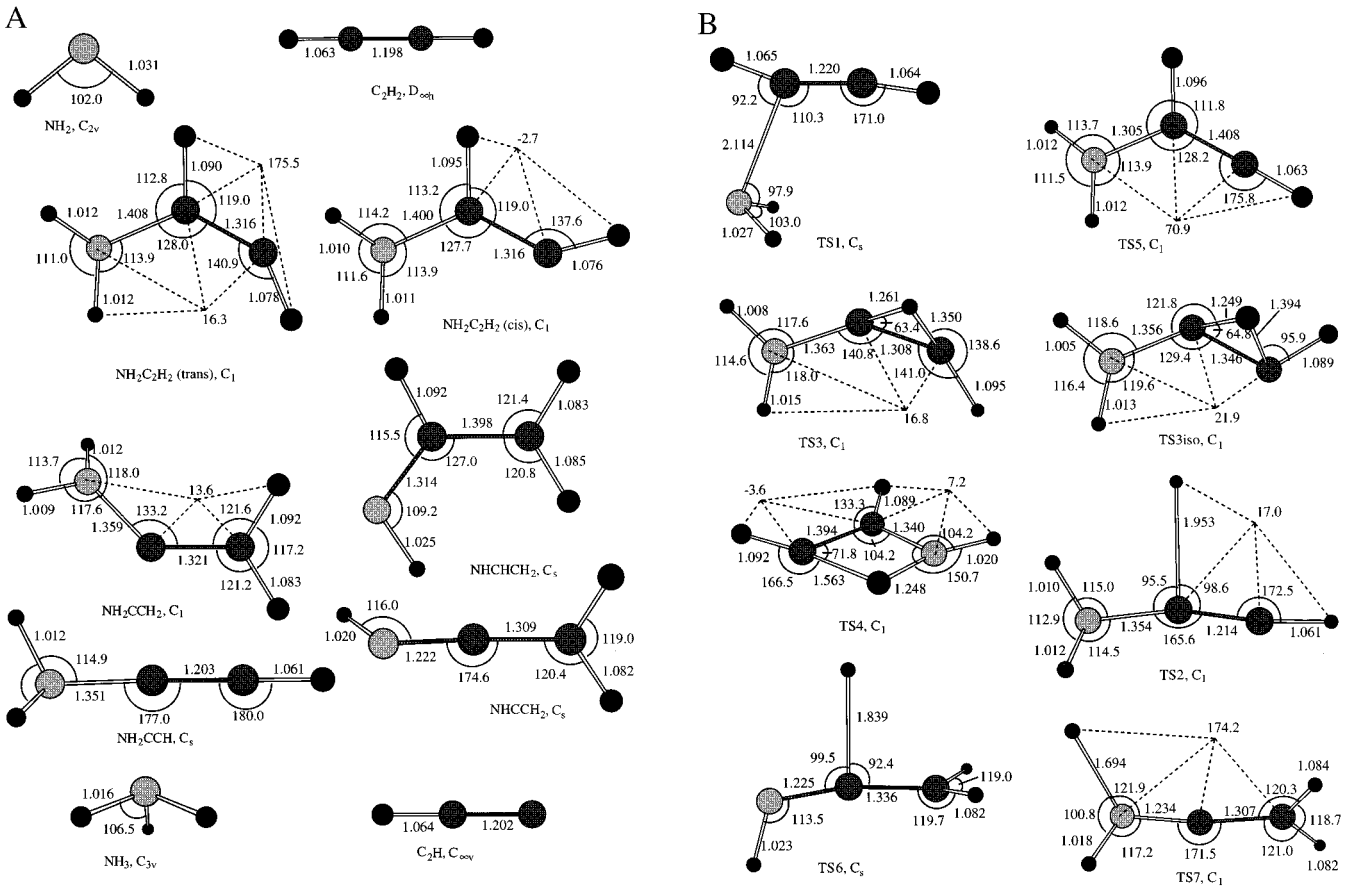

Figure 1. (A) Optimized (B3LYP) geometries of the various species involved in the reaction of the NH_2 radical with acetylene. (B) Optimized (B3LYP) geometries of the various transition states involved in the reaction of the NH_2 radical with acetylene.

where

$$\Delta E(+) = E[\text{PMP4/6-311+G(d,p)}] - E[\text{PMP4/6-311G(d,p)}]$$

$$\Delta E(\text{2df,p}) = E[\text{PMP4/6-311G(2df,p)}] - E[\text{PMP4/6-311G(d,p)}]$$

$$\Delta E(\text{RCC}) = E[\text{RCCSD(T)/6-311G(d,p)}] - E[\text{PMP4/6-311G(d,p)}]$$

$$\Delta' = E[\text{MP2/6-311+G(3df,2p)}] - E[\text{MP2/6-311G(2df,p)}] - E[\text{MP2/6-311+G(d,p)}] + E[\text{MP2/6-311G(d,p)}]$$

$$\Delta E(\text{HLC}) = -5.71n_\beta - 0.19n_\alpha$$

where n_α and n_β are the numbers of α and β valence electrons, respectively, and the numerical coefficients are given in units of mhartree.

The frequencies and ZPE calculated at the B3LYP/6-311G-(d,p) level were used without scaling. All the molecular orbital calculations were performed with the GAUSSIAN94 program package[8] except those of RCCSD(T), which were carried out using the MOLPRO96[9] program.

B. Multichannel RRKM Calculations. The effects of temperature and pressure on the rate of the $NH_2 + C_2H_2$ reaction were examined for the lowest energy path (Figure 3) with the inclusion of the deactivation of the chemically activated adducts denoted by †:

$$NH_2 + C_2H_2 \underset{-a}{\overset{a}{\rightleftharpoons}} \text{t-}H_2NCHCH^\dagger \underset{-b}{\overset{b}{\rightleftharpoons}} \text{c-}H_2NCHCH^\dagger \xrightarrow{c} H_2NC_2H + H \quad (1)$$

$$\text{t-}H_2NC_2H_2^\dagger + M \rightarrow \text{t-}H_2NC_2H_2 + M \quad (2)$$

$$\text{c-}H_2NC_2H_2^\dagger + M \rightarrow \text{c-}H_2NC_2H_2 + M \quad (3)$$

Several multichannel, coupled systems of this type have been treated in this laboratory earlier, e.g., the reaction of NH_2 with NO producing OH + HN_2 and H_2O + N_2 via two long-lived intermediates, H_2NNO and HNNOH.[14] The same computer program employed for the NH_2 + NO reaction was used in the present calculation.

III. Results and Discussion

The geometries of the reactants, intermediates, products, and connecting transition states are summarized in Figure 1(A) and (B). The schematic potential energy profile of the entire system is shown in Figure 2. The computed energetics by various methods and the molecular parameters for the species relevant to RRKM calculations are presented in Tables 1 and 2, respectively. Here, and in the discussion below, all the energies are related to the reactants, unless otherwise noted.

A. Reaction of Amidogen with Acetylene. Two options are open for the first reaction step, namely, addition to the triple bond and the abstraction of a hydrogen atom by the NH_2 radical.

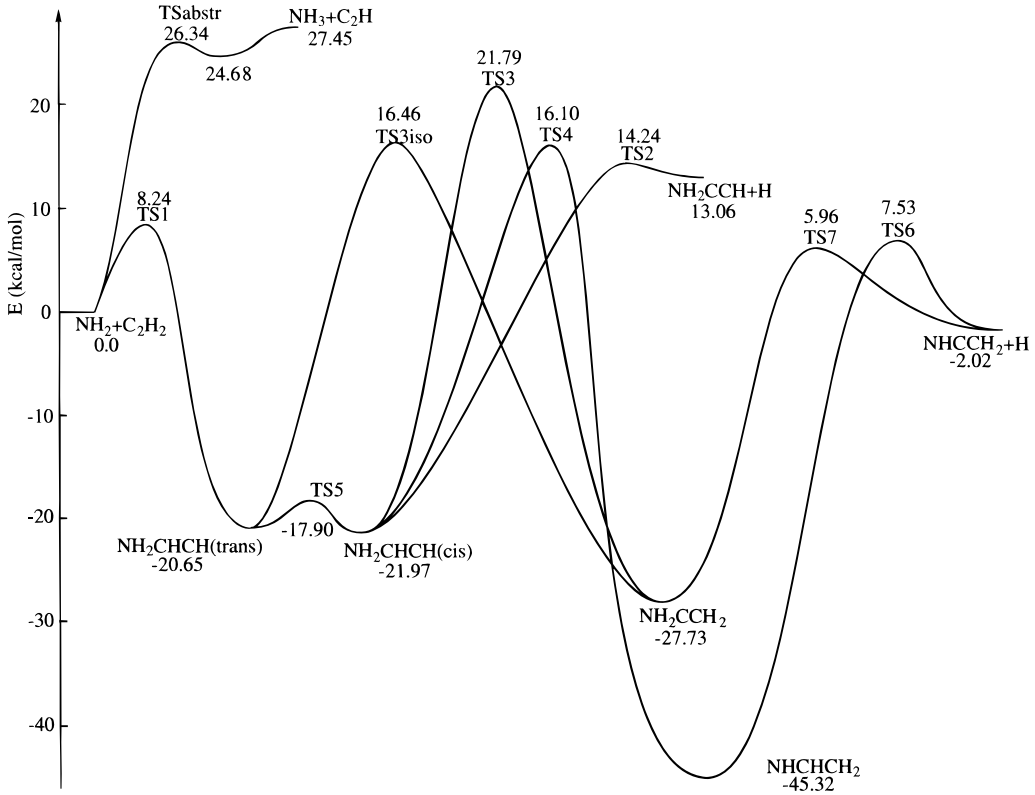

Figure 2. Schematic energy diagram for the potential energy surface of the $NH_2 + C_2H_2$ reaction. Energies are obtained from the G2M(RCC) calculation.

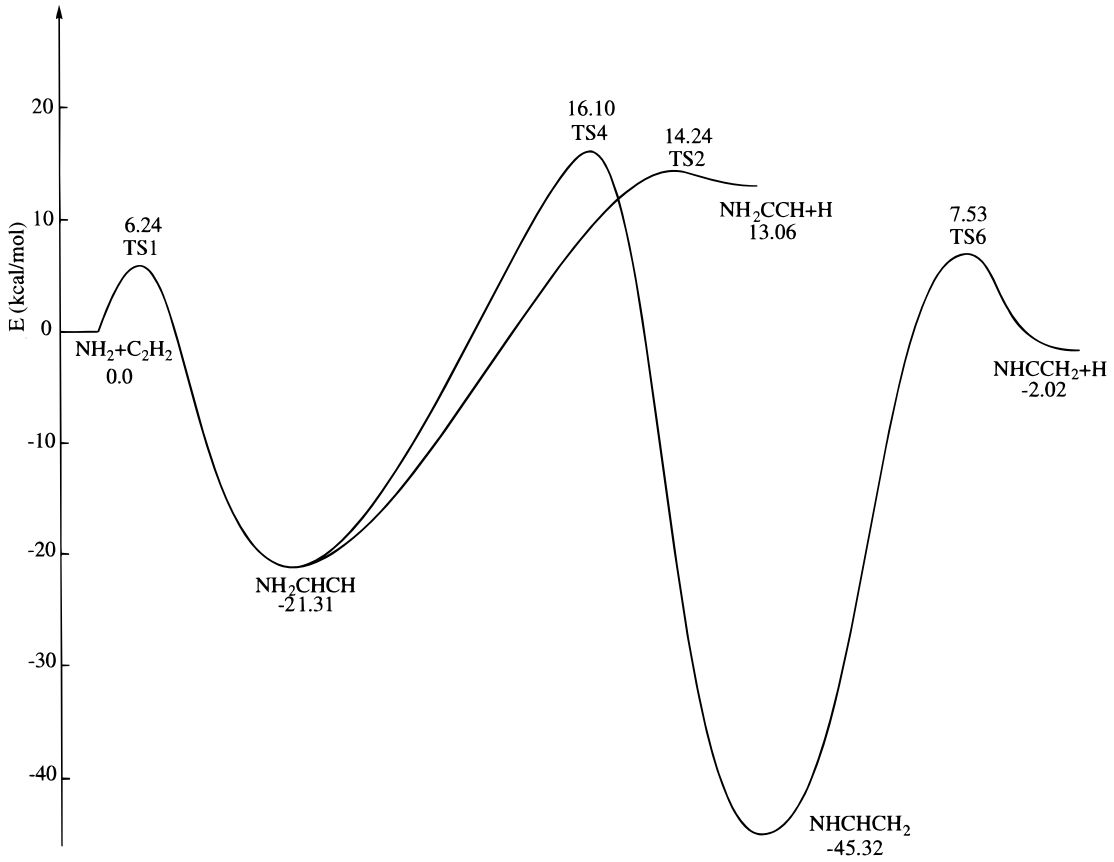

Figure 3. Lowest energy path used in RRKM calculations on the $NH_2 + C_2H_2$ system.

The latter is shown to have a high barrier of 26.34 kcal/mol and is, therefore, of minor importance for the reaction kinetics. Our investigation has thus been focused on the addition channel and the further transformations of the adduct.

The transition state for NH_2 addition to C_2H_2, represented on the diagram as TS1, lies 8.24 kcal/mol above the reactants at our G2M(RCC) level. It has C_s symmetry, the two hydrogen atoms of the amino group being out of plane. However, in the

TABLE 1: Relative Energies (ZPE-Corrected, in kcal/mol) for Species and Transition States Involved in the Reaction of Amino Radical with Acetylene

species and transition states	ZPE[a]	B3LYP/6-311G(d,p)	UMP2/6-311+G(3df,2p)	PMP4/6-311G(2df,p)	RCCSD(T)/6-311G(d,p)	G2M(RCC)
$NH_2(^2B_1) + C_2H_2(^1\Sigma_g^+)$[b]	28.76	0.00	0.00	0.00	0.00	0.00
TSabstr	30.47	18.64	37.28	25.42	25.63	26.34
$NH_3(^1A_1) + C_2H(^2\Sigma^+)$	30.37	28.86	38.69	29.89	27.04	27.45
TS1	31.16	4.55	16.65	6.57	8.56	8.24
trans-$NH_2C_2H_2$	34.48	−24.21	−17.25	−20.31	−19.81	−20.65
cis-$NH_2C_2H_2$	34.47	−25.38	−18.7794	−21.48	−20.98	−21.97
TS5	33.37	−22.50	−17.90	−18.13	−16.58	−17.90
TS2	28.71	14.66	15.65	16.01	19.99	14.24
$NH_2CCH(^1A') + H$	27.77	12.02	5.18	10.26	13.98	13.06
TS3	30.76	16.39	19.61	21.12	24.12	21.79
TS3iso	31.74	11.94	16.77	17.45	18.80	16.46
$NH_2CCH_2(^1A')$	34.38	−32.93	−24.70	−26.24	−26.63	−27.73
TS4	30.47	9.68	17.18	13.55	16.34	16.10
$NHCHCH_2$	34.46	−50.15	−38.77	−47.85	−45.78	−45.32
TS6	28.21	1.18	8.88	3.99	8.16	7.53
TS7	28.51	−2.58	3.78	2.73	6.40	5.96
$NHCCH_2(^1A') + H$	27.42	−0.64	−7.77	−5.41	−1.85	−2.02

[a] ZPE is calculated at the B3LYP/6-311G(d,p) level. [b] The total energies (in hartree) for the $NH_2 + C_2H_2$ system are B3LYP/6-311G(d,p), −133.2498; MP2/6-311G(d,p), −132.84799; MP4/6-311G(d,p), −132.89817; MP2/6-311+G(d,p), −132.85455; MP4/6-311+G(d,p), −132.9047; MP2/6-311G(2df,p), −132.90969; MP4/6-311G(2df,p), −132.96359; MP2/6-311+G(3df,2p), −132.93016; RCCSD(T)/6-311G9d,p), −132.89761.

adduct, the hybridization changes to sp^2; that is, the geometry of the N-center is almost planar and twisted relative to the TS structure, so that the C_s symmetry is not preserved. This symmetry breakdown at some point along the reaction coordinate is causing splitting of the path or double path degeneracy on going from the product to TS1. To be accurate, we carried out an IRC procedure which enabled us to observe the geometry change in the course of the reaction. An IRC (intrinsic reaction coordinate) analysis revealed additionally that the product formed has trans-structure in the outermost CH bond orientation. However, we were unable to locate any other transition state different from TS1 that would relate the alternative cis-structure and the reactants.

The geometries of the two isomers are similar (with the exception of one angle) and so are their energies, −20.65 and −21.97 kcal/mol relative to the reactants, the deeper minimum corresponding to cis-isomer. The conversion barrier is small, less than 3 kcal/mol from trans to cis. Therefore, at moderately high temperatures the interchange occurs fast enough to render the two structures indistinguishable.

B. Hydrogen Atom Migration. We considered two possibilities for the hydrogen atom migration to form more stable radicals $NH_2-C{=}CH_2$ and $NH-CH{=}CH_2$. The latter is remarkably stabilized by electronic resonance (its energy is 24.67 kcal/mol lower compared to *trans*-$NH_2C_2H_2$). The two corresponding transition states (defined as TS3iso and TS4) have close energies, 16.46 and 16.10 kcal/mol above the reactants, respectively, the former being linked to the trans-isomer whereas the latter is allied with the cis-isomer. $NH_2C{=}CH_2$ product can be formed from the cis-intermediate as well; this process refers to TS3 and requires much higher activation energy.

C. Dehydrogenation. At high temperatures, all radical intermediates are expected to lose a hydrogen atom, forming stable molecules. Kicking off the hydrogen atom from *cis*-$NH_2-CH{=}CH$ produces aminoacetylene $NH_2-C{\equiv}CH$. Similarly to the NH_2 addition to the triple bond of acetylene, H addition to $NH_2-C{\equiv}CH$ occurs stereospecifically; that is, only *cis*-$NH_2-CH{=}CH$ is formed. This was confirmed by IRC reaction path analysis. The corresponding barrier height for the forward reaction is 36.21 kcal/mol. The hydrogen atom loss by the two other intermediates, NH_2CCH_2 and $NHCHCH_2$, leads to an isomeric product, $HN{=}C{=}CH_2$, which is 15.08 kcal/mol more stable than its counterpart. In fact, NH_2CCH_2 can also decompose to $NH_2-C{\equiv}CH$, but because of high endothermicity, this channel is not important to the overall reaction rate.

D. Rate Constants for the Reaction via the Lowest Energy Paths. The lowest energy paths for the reaction of NH_2 with C_2H_2 and the decomposition of the $H_2NC_2H_2$ (cis + trans) adducts are depicted in Figure 3. Because of the small energetic and structural difference between the *cis*- and *trans*-$H_2NC_2H_2$ isomers, these two adducts were treated to be the same, and only a single well was assumed in our RRKM calculations.

The rate constant for the disappearance of the NH_2 radical in the presence of an excess amount of C_2H_2, as employed under all pseudo-first-order conditions, is controlled primarily by the addition step (a) via TS1 at low temperatures and at pressures greater than 10 Torr (as in the studies by Bosco[13] and Lesclaux[10] and their co-workers). At lower pressures, employed in Hack's experiment ($p = 1$ Torr), the redissociation of the excited adduct $H_2NC_2H_2^\dagger$ becomes competitive with the deactivation process. The measured rate constant is thus pressure-dependent.

The pressure dependency becomes greater when the temperature of the system increases because of the increasing redissociation rate. The pressure effect is expected to diminish when the temperature of the system reaches that of the shock tube study by Wagner and co-workers, $T > 1500$ K, because of the accessibility of higher energy decomposition channels producing H atoms via the direct decomposition and indirect isomerization/decomposition channels as shown in Figure 3.

The calculated rate constants for the disappearance of NH_2 at different pressures have been fitted to the following Arrhenius equations:

$$k^\infty = 1.46 \times 10^7 T^{1.67} e^{-2559/T} \quad 250\ \text{K} \le T \le 500\ \text{K}$$

$$k^\infty = 6.76 \times 10^{13} T^{-0.2} e^{-4689/T} \quad 500\ \text{K} \le T \le 2000\ \text{K}$$

$$k(350\ \text{Torr}) = 3.74 \times 10^{22} T^{-3.97} e^{-3779/T} \quad 250\ \text{K} \le T \le 500\ \text{K}$$

$$k(350\ \text{Torr}) = 7.65 \times 10^{-18} T^{8.31} e^{3740/T} \quad 500\ \text{K} \le T \le 2000\ \text{K}$$

$$k(1\ \text{Torr}) = 2.01 \times 10^{15} T^{-2.37} e^{-2964/T} \quad 250\ \text{K} \le T \le 500\ \text{K}$$

TABLE 2: Molecular and Transition-State Parameters Used for RRKM Calculations on the $NH_2 + C_2H_2$ System

species or transition state	E_{rel}[a] (kcal/mol)	$I_aI_bI_c \times 10^{117}$ (g^3 cm^6)[b]	ν (cm^{-1})		species or transition state	E_{rel}[a] (kcal/mol)	$I_aI_bI_c \times 10^{117}$ (g^3 cm^6)	ν (cm^{-1})	
NH_2		0.009102	1536		TS4	16.1	114.3	1761i	1159
			3328					49	1382
			3414					646	1410
								798	2034
								933	3103
								1011	3144
								1077	3460
								1110	
C_2H_2		0.5631[b]	643		$NHCHCH_2$	−45.32	99.23	491	1378
			643					493	1452
			774					682	1499
			774					826	3096
			2060					988	3132
			3420					1077	3235
			3523					1140	3383
								1238	
TS1	6.24	264.5	435i	826	TS6	7.53	92.39	947i	1042
			162	1548				28	1119
			264	1913				460	1425
			536	3375				564	2028
			611	3398				603	3156
			691	3468				730	3248
			742	3481				884	3440
			780					1007	
$NH_2C_2H_2$ (average of cis and trans)	−21.31	100.7	327	1331	TS2	14.25	89.89	616i	1078
			449	1645				178	1198
			559	1673				423	1632
			672	3104				458	2165
			798	3262				497	3479
			884	3527				524	3534
			1070	3628				596	3627
			1193					690	

[a] Energies relative to the reactants are given as calculated by G2M(RCC)//B3LYP/6-311G(d,p), except the TS1, for which the energy was lowered by 2 kcal/mol; the geometries and vibrational frequencies are computed at the B3LYP/6-311G(d,p) level of theory. [b] For the acetylene molecule we give $I_aI_b \times 10^{77}$ in g^2 cm^3 ($I_c = 0$).

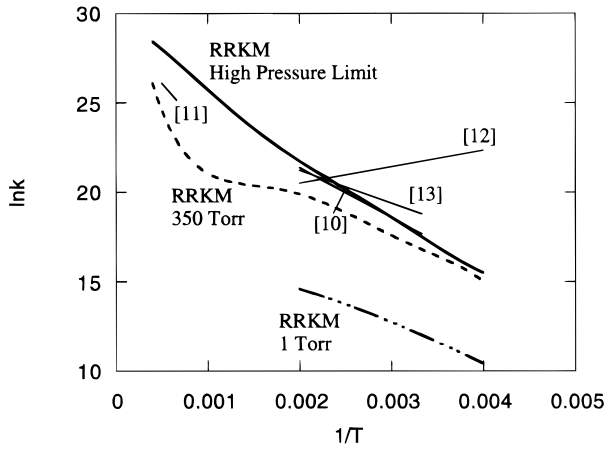

Figure 4. Arrhenius plot of rate data for the reaction $NH_2 + C_2H_2$. RRKM result with the ab initio barrier lowered by 2.0 kcal/mol; [10], [12], [11], and [13] are experimental data.

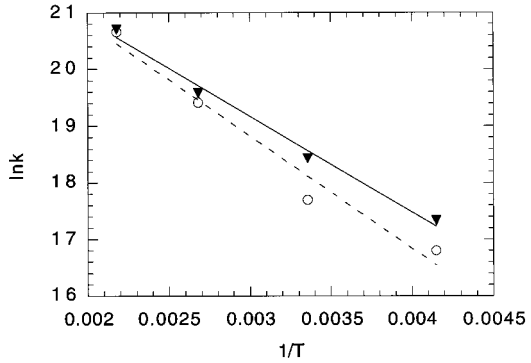

Figure 5. Kinetic modeling of the $C_2H_2 + NH_2$ reaction under Bosco conditions (25 Torr): (▼) Bosco;[13] (○) modeling result. Rate constants are given in $cm^3 \cdot mol^{-1} \cdot s^{-1}$.

and are also presented in Figure 4 in comparison with experimental data. To quantitatively account for the low-temperature data of Bosco et al.[13] and Lesclaux and co-workers[10] (they are in close agreement), the calculated addition barrier was lowered from 8 to 6 kcal/mol. The result of Hack et al.[12] obtained at 1 Torr He pressure with negative activation could not be reasonably accounted for, however. The apparent large deviation between theory and experiment, particularly that of Hack, results from the combination of pressure and secondary reaction effects.

In the Appendix, we summarize the results of kinetic modeling of NH_2 decay rates employing experimental conditions reported by these authors. Using the predicted rate constant calculated at 1 Torr pressure, we found that Hack's NH_2 decay rates were enhanced significantly by fast side reactions such as $NH_2 + NH_2$ and $NH_2 + NH_2C_2H_2$.

We have also examined the effects of secondary reactions on the results of Bosco[13] and Lesclaux[10] under individual experimental conditions. Surprisingly, both sets of data obtained under the $[C_2H_2] \gg [NH_2]$ pseudo-first-order conditions were not immune to the effects, particularly at lower temperatures, at which the addition reaction became slower and the faster radical−radical reactions became competitive despite their lower concentrations, because the kinetically modeled rate constants for NH_2 decay exhibit 1−2 kcal/mol higher activation energies than originally reported (see Figures 5−7 and the discussion in the Appendix for detail).

TABLE 3: Mechanisms Used for the $NH_2 + C_2H_2$ Reaction[a]

reaction	*A*	*B*	*C*	remarks
	Modeling under Bosco[13] Conditions			
1. $NH_2 + C_2H_2 = NH_2C_2H_2$	5.80×10^{10}	0.0	1986.7	*b*
2. $NH_2 + NH_2 + M = N_2H_4 + M$	1.00×10^{19}	0.0	0.0	19
3. $C_2H_2 + H + M = C_2H_3 + M$	1.90×10^{19}	0.0	1470.0	18
4. $C_2H_2 + H = H_2 + C_2H$	6.02×10^{13}	0.0	27821.0	18
5. $C_2H_3 + NH_2 = NH_3 + C_2H_2$	1.00×10^{13}	0.0	0.0	*c*
	Modeling under Lesclaux[10] Conditions			
1. $NH_2 + C_2H_2 = NH_2C_2H_2$	2.64×10^{12}	0.0	3612.8	*b*
2. $NH_2 + NH_2 = N_2H_4$	1.50×10^{13}	0.0	0.0	19
3. $NH_2 + NH_2 = NH_3 + NH$	2.50×10^{13}	0.0	0.0	17
4. $NH_2C_2H_2 + NH_2 \rightarrow NH_2C_2H_2NH_2$	1.00×10^{13}	0.0	0.0	*c*
5. $NH_2C_2H_2 + NH_2 \rightarrow NH_2C_2H + NH_3$	5.00×10^{12}	0.0	0.0	*c*
6. $NH_2C_2H_2 + H \rightarrow NH_2C_2H_3$	1.00×10^{13}	0.0	0.0	*c*
7. $NH_2C_2H_2 + C_2H_2 \rightarrow NH_2C_4H_4$	5.00×10^{5}	0.0	0.0	*c*
8. $C_2H_2 + H = C_2H_3$	5.55×10^{12}	0.0	2410.0	16
9. $C_2H_2 + H = H_2 + C_2H$	6.02×10^{13}	0.0	27821.0	2
10. $C_2H_3 + NH_2 \rightarrow NH_2C_2H_3$	1.00×10^{13}	0.0	0.0	*c*
11. $C_2H_3 + NH_2 = NH_3 + C_2H_2$	1.00×10^{13}	0.0	4000.0	*c*
12. $C_2H_3 + NH = NH_2 + C_2H_2$	1.00×10^{13}	0.0	5000.0	*c*
13. $NH_2 + H = NH_3$	6.00×10^{12}	0.0	0.0	*c*
14. $NH_2 + H = NH + H_2$	4.00×10^{13}	0.0	3650.0	15
15. $H + H + M = H_2 + M$	7.31×10^{17}	−1.0	0.0	18
16. $NH_2 + C_2H = NH + C_2H_2$	1.00×10^{13}	0.0	4000.0	*c*
	Modeling under Hack[12] Conditions			
1. $NH_2 + C_2H_2 = NH_2C_2H_2$	2.30×10^{8}	0.0	2255.3	*d*
2. $NH_2 + NH_2 + M = N_2H_4 + M$	1.00×10^{19}	0.0	0.0	19
3. $NH_2 + NH_2 = NH_3 + NH$	2.50×10^{13}	0.0	0.0	17
4. $NH_2C_2H_2 + NH_2 \rightarrow NH_2C_2H_2NH_2$	1.00×10^{13}	0.0	0.0	*c*
5. $NH_2C_2H_2 + NH_2 \rightarrow NH_2C_2H + NH_3$	5.00×10^{12}	0.0	0.0	*c*
6. $NH_2C_2H_2 + C_2H_2 \rightarrow NH_2C_4H_4$	5.00×10^{5}	0.0	0.0	*c*
7. $NH_2 + H = NH_3$	1.00×10^{12}	0.0	0.0	*c*
8. $NH_2 + C_2H = NH + C_2H_2$	1.00×10^{13}	0.0	4000.0	*c*

[a] The rate constants are given by $k = AT^Be^{-C/T}$ in units of cm^3, mol, and s. [b] The rate constants were obtained by fitting to NH_2 decays observed in the corresponding experimental studies. [c] Assumed. [d] RRKM prediction for 1 Torr.

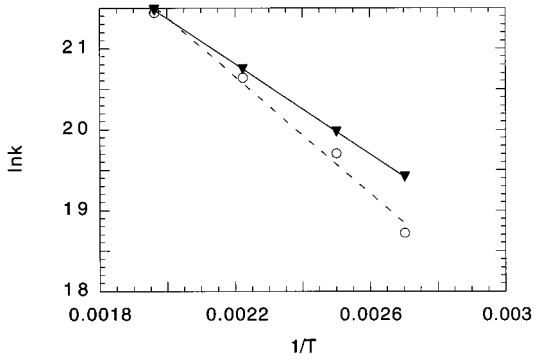

Figure 6. Kinetic modeling of the $C_2H_2 + NH_2$ reaction under Lesclaux conditions (50 Torr): (▼) Lesclaux;[10] (○) modeling result. Rate constants are given in $cm^3 \cdot mol^{-1} \cdot s^{-1}$.

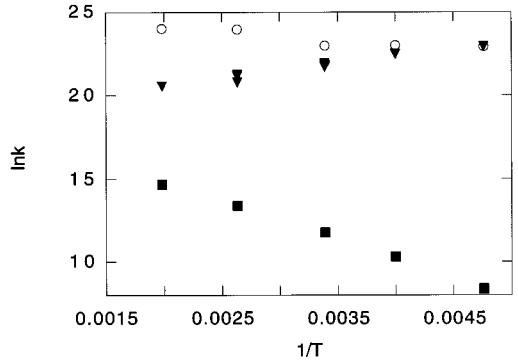

Figure 7. Kinetic modeling of the $C_2H_2 + NH_2$ reaction under Hack conditions (1 Torr): (▼) Hack;[12] (■) RRKM; (○) modeling result. Rate constants are given in $cm^3 \cdot mol^{-1} \cdot s^{-1}$.

The theoretically calculated results presented for 350 Torr Ar duplicating the condition employed by Hennig and Wagner[11] exhibit a strong nonlinear behavior because of the redissociation of $NH_2C_2H_2$ at moderate temperatures (800−1200 K), beyond which the value of the rate constant turns up sharply, resulting from the opening of the exit channels as mentioned above. The predicted value in the 1500−2000 K region agrees reasonably with the measured result of Hennig and Wagner. Under high-temperature conditions, the NH_2-for-H displacement process

$$NH_2 + C_2H_2 \rightleftharpoons NH_2C_2H_2^{\dagger} \rightarrow NH_2C_2H + H \qquad (4)$$

becomes dominant, as illustrated in Figure 4. A similar observation was made for the isoelectronic $CH_3 + C_2H_2$ reaction.[21]

To complete the analysis, we employed a tunneling correction for the high energetic channels b and c (eq 1). This test revealed tunneling effects on the overall rate to be negligible.

IV. Conclusion

We performed a detailed investigation of the $NH_2 + C_2H_2$ reaction mechanism combining high-level MO and statistical theory calculations. The calculated barrier for the addition step is 8.24 kcal/mol at the G2M(RCC) level. With the exception of the NH_2-for-H displacement products, $NH_2C_2H + H$ and $NHCCH_2$, all adducts and their isomers, $NH_2C_2H_2$ (−HCCH-trans and −HCCH-cis) were found to be more stable than the reactants, $NH_2 + C_2H_2$. Therefore, the reaction is expected to produce predominantly these isomeric products.

Multichannel RRKM calculations were carried out for the lowest energy path including hydrogen loss by the adduct or

its isomerization to allyl analogue, $NHCHCH_2$, followed by dissociation to form $NHCCH_2 + H$. The low conversion barrier between cis- and trans-adducts enabled us to treat them as a single well. Our calculation reveals that the rate constant for the NH_2 disappearance is controlled primarily by the addition step. The reaction rate is expected to be pressure-dependent due to the increased redissociation rate of the activated adduct at low pressures. The pressure effect is diminished at temperatures above 1000 K because of the accessibility of higher energy decomposition channels and indirect isomerization/decomposition channels.

Kinetic modeling performed under experimental conditions reveals a substantial effect of secondary reactions on the observed NH_2 decay rates. This explains the large scatter in the reported rate constants and activation energies obtained under varying experimental conditions.

Acknowledgment. The authors gratefully acknowledge the support received from the Department of Energy, Office of Basic Energy Sciences, Division of Chemical Sciences, through Contract DE-FGO2-97ER14784. Also, we are thankful to the Cherry L. Emerson Center for Scientific Computation for the use of various programs and computing facilities.

Appendix. Modeling of the NH_2 Decay Rates under Various Experimental Conditions

We attempted to model the effect of secondary reactions on the NH_2 decay rates for the three sets of experimental data by Bosco et al.,[13] Lesclaux et al.,[10] and Hack et al.[12] to account for the effective lower activation energy as compared to the theoretical prediction.

In the study of Bosco et al., the NH_2 decay was measured by the flash photolysis technique combined with time-resolved detection of NH_2 via laser-induced fluorescence under $[C_2H_2] \gg [NH_2]$ conditions with $[NH_2]_0$ estimated as $\sim 5 \times 10^{10}$ molecule·cm^{-3} at a typical 1 Torr ammonia partial pressure and 10−100 Torr total pressure. The modeling was performed for 25 Torr total pressure with the mechanism given in Table 3, where the rate of reaction 1 was varied to fit the experimentally observed decay rates (under the reported pseudo-first-order conditions). Our modeling (see Figure 5) predicts a steeper slope for the disappearance of NH_2 via the addition step, with the activation energy of 3.95 kcal/mol comparing with the reported value of 3.36 kcal/mol.

In a similar manner, we modeled the experiment by Lesclaux et al.,[10] who also used flash photolysis combined with the laser resonance absorption technique. In that study, the initial concentration of the NH_2 radical was $\sim 2.5 \times 10^{12}$ molecule·cm^{-3}. Acetylene was used as a bath gas. Therefore, in the mechanism (Table 3) the acetylene secondary reactions are playing an important role. We have modeled several points at 50 Torr total pressure and observed a substantial effect of secondary reactions, as illustrated in Figure 6.

Hack et al.[12] measured the NH_2 decay in about the same region as the two studies discussed above, but at lower pressures (∼1 Torr) using a discharge flow system with the laser-induced resonance fluorescence detection of NH_2, which was generated in the $F + NH_3 \rightarrow HF + NH_2$ reaction. The modeling based on the RRKM-predicted (for 1 Torr) rate constant shows an enormous deviation due to side reactions (Figure 7). Our preliminary ab initio calculation predicts the formation of the $NH_2 \cdots HF$ molecular complex, which is 9.7 kcal/mol [B3LYP/6-311G(d,p) level] more stable than the isolated species. This may affect the observed NH_2 decay rate as well.

References and Notes

(1) Miller, J. A.; Bowman, C. T. *Prog. Energy Combust. Sci*. **1989**, *15*, 287.

(2) (a) Kaye, J. A.; Strobel, D. F. *Icarus* **1983**, *54*, 417. (b) Strobel, D. F. *Int. Rev. Phys. Chem*. **1983**, *3*, 145.

(3) Young, Y. L.; Allen, M.; Pinto, J. P. *Astrophys. J. Suppl. Ser*. **1984**, *55*, 465.

(4) (a) Curtiss, L. A.; Raghavachari, K.; Trucks, G. W.; Pople, J. A. *J. Chem. Phys*. **1991**, *94*, 7221. (b) Pople, J. A.; Head-Gordon, M.; Fox, D. J.; Raghavachari, K.; Curtiss, L. A. *J. Chem. Phys*. **1989**, *90*, 5622. (c) Curtiss, L. A.; Jones, C.; Trucks, G. W.; Raghavachari, K.; Pople, J. A. *J. Chem. Phys*. **1990**, *93*, 2537.

(5) Mebel, A. M.; Morokuma, K.; Lin, M. C. *J. Chem. Phys.* **1995**, *103*, 7414.

(6) (a) Becke, A. D. *J. Chem. Phys*. **1993**, *98*, 5648. (b) *J. Chem. Phys*. **1992**, *96*, 2155. (c) *J. Chem. Phys*. **1992**, *97*, 9173.

(7) Lee, C.; Yang, W.; Parr, R. G. *Phys. Rev. B* **1988**, *37*, 785.

(8) Frisch, M. J.; Trucks, G. W.; Schlegel, H. B.; Gill, P. M. W., Johnson, B. G., Robb, M. A.; Cheeseman, J. R.; Keith, T.; Petersson, G. A.; Montgomery, J. A.; Raghavachari, K.; Al-Laham, M. A.; Zakrzewski, V. G.; Ortiz, J. V.; Foresman, J. B.; Cioslowski, J.; Stefanov, B. B.; Nanayakkara, A.; Challacombe, M.; Peng, C. Y.; Ayala, P. Y.; Chen, W.; Wong, M. W.; Andres, J. L.; Replogle, E. S.; Gomperts, R.; Martin, R. L.; Fox, D. J.; Binkley, J. S.; Defrees, D. J.; Baker, J.; Stewart, J. P.; Head-Gordon, M.; Gonzalez, C.; Pople, J. A. *GAUSSIAN 94*, Revision A.1; Gaussian, Inc.: Pittsburgh, PA, 1995.

(9) MOLPRO is a package of ab initio programs written by Werner, H.-J.; Knowles, P. J. with contributions from Almlöf, J.; Amos, R. D.; Deegan, M. J. O.; Elbert, S. T.; Hampel, C.; Meyer, W.; Peterson, K.; Pitzer, R.; Stone, A. J.; Taylor, P. R. Open-shell coupled-cluster (RCCSD): Knowles, P. J.; Hampel C.; Werner, H.-J. *J. Chem. Phys*. **1993**, *99*, 5219.

(10) Lesclaux, R.; Veyret, B.; Roussel, P. *Ber. Bunsen-Ges. Phys. Chem.* **1985**, *89*, 330.

(11) Hennig, G.; Wagner, H. Gg. *Ber. Bunsen-Ges. Phys. Chem*. **1995**, *99*, 989.

(12) Hack, W.; Schacke, H.; Schröter, M.; Wagner, H. Gg. *17th Symp. (Int.) Combust.* **1979**, 505.

(13) Bosco, S. R.; Nava, D. F.; Brobst, W. D.; Stief, L. J. *J. Chem. Phys.* **1984**, *81*, 3505.

(14) Diau, E. W. G.; Yu, T.; Wagner, M. A. G.; Lin, M. C. *J. Phys. Chem.* **1994**, *98*, 4034.

(15) Davidson, D. F.; Kohse-Hoinghaus, K.; Chang, A. Y.; Hanson, R. K. *J. Chem. Kinet*. **1990**, *22*, 513.

(16) Payne, W. A.; Stief, L. J. *J. Chem. Phys*. **1976**, *64*, 1150.

(17) Diesen, R. W. *J. Chem. Phys*. **1963**, *39*, 2128.

(18) Baulch, D. L.; Cobos, C. J.; Cox, R. A.; Esser, C.; Frank, P.; Just, Th.; Kerr, J. A.; Pilling, M. J.; Troe, J.; Walker, R. W.; Warnatz, J. *J. Phys. Chem. Ref. Data* **1992**, *21*, 411.

(19) Khe, P. V.; Soulignac, J. C.; Lesclaux, R. *J. Phys. Chem.*, **1977**, *81*, 210.

(20) Dransfeld, P.; Hack, W.; Kurzke, H.; Temps, F.; Wagner, H. G. *20th Symp. Int. Combust. Proc.* **1985**, *20*, 655.

(21) Diau, E. W. G.; Lin, M. C.; Melius, C. F. *J. Chem. Phys.* **1994**, *101*, 3923.